Review Article

Azimuthally Integrated HBT Parameters for Charged Pions in Nucleus-Nucleus Interactions versus Collision Energy

V. A. Okorokov

National Research Nuclear University "MEPhI" (Moscow Engineering Physics Institute), Kashirskoe Shosse 31, Moscow 115409, Russia

Correspondence should be addressed to V. A. Okorokov; vaokorokov@mephi.ru

The energy dependence of spatiotemporal characteristics of particle emission region is studied for charged pions produced in nuclear collisions. No dramatic change is observed for the HBT parameters with increasing of the center-of-mass (c.m.) energy per nucleon-nucleon pair, $\sqrt{s_{NN}}$, for $\sqrt{s_{NN}}$ of a few GeV to a few TeV. The emission duration is obtained to be almost independent of the c.m. energy within the measurement uncertainties. The analytic function is suggested for a smooth approximation of the energy dependence of the main HBT parameters. The fits demonstrate reasonable agreement with the experimental data. Predictions are made for future LHC and FCC experiments.

1. Introduction

At present, two-particle interferometry analysis (often referred to as HBT) in particular that is based on Bose-Einstein correlations is a unique experimental method for determination of sizes and lifetime of particle source in high energy and nuclear physics. Space-time characteristics for emission region of secondary particles created in (heavy) ion collisions are important for study of deconfinement state of strongly interacting matter, strong-coupling quark-gluon plasma (sQGP). Furthermore, the study of energy dependence of HBT observables can be useful for understanding in detail the transition from sQGP produced at higher energies to confined hadronic resonance matter created in final state at lower energies. HBT analysis allows studying dynamic features of interaction process at late, that is, soft, stage of space-time evolution of multiparticle final state. Therefore, the study of nucleus-nucleus collisions in wide energy domain by HBT correlations seems important for better understanding of both the equation of state (EOS) of strongly interacting matter and general dynamic features of soft processes.

The paper is organized as follows. In Section 2, definitions of main observables for analysis of two-pion correlations are briefly described. Section 3 is devoted to discussion of experimental energy dependence for space-time extent of source of charged pions and corresponding fits. Also estimations for HBT observables are shown for the LHC and the future circular collider (FCC) project energies. Some final remarks and conclusions are presented in Section 4.

2. Method and Variables

In general, phenomenological parameterization of correlation function (CF) for two identical particles with 4-momenta p_1, p_2 taking into account different forms of corrections on Coulomb final state interaction (FSI) can be written as follows [1]:

$$C_{2,(m)}^{ph}(q, K) = \epsilon P_{coul}^{(m)}(q)\left[\epsilon^{-1} + \mathbf{K}_2^{ph}(\mathbf{A})\right],$$
$$\epsilon = \begin{cases} \lambda, & \text{at } m = 1, 2; \\ 1, & \text{at } m = 3, \end{cases} \tag{1}$$

where $m = 1$ corresponds to the standard Coulomb correction, $m = 2$ the dilution procedure, and $m = 3$ the Bowler-Sinyukov correction; $q \equiv (q^0, \vec{q}) = p_1 - p_2$ is the relative 4-momentum and $K \equiv (K^0, \vec{K}) = (p_1 + p_2)/2$ the average

4-momentum of particles in pair (pair 4-momentum), for the standard simplest (Gaussian) case:

$$\mathbf{K}_2^{\mathrm{ph}}(\mathbf{A}) = \prod_{i,j=1}^{3} \mathbf{K}_2^{\mathrm{ph}}\left(A_{ij}\right) = \exp\left(-\sum_{i,j=1}^{3} q_i R_{ij}^2 q_j\right). \quad (2)$$

Here $\mathbf{A} \equiv \vec{q}\mathbf{R}^2\vec{q}^T$ and $\mathbf{R}^2$ are the matrices 3×3 and $\vec{q}^T$ is transposed vector $\vec{q}$, $\forall i,j : R_{ij}^2 = R_{ji}^2$, $R_{ii}^2 \equiv R_i^2$, where $R_i = R_i(K)$ are parameters that characterized the linear scales of homogeneity region [2]; the products are taken on space components of vectors; $\lambda(K) = \mathbf{K}_2(0,K)$, $0 \leq \lambda \leq 1$, is the parameter which characterizes the degree of source chaoticity. Different types of Coulomb correction for two-pion correlations are compared in [1]. The space component of pair 4-momentum $(\vec{K})$ is decomposed on longitudinal $k_{\parallel} = (p_{\parallel,1} + p_{\parallel,2})/2$ and transverse $\vec{k}_{\perp} = (\vec{p}_{\perp,1} + \vec{p}_{\perp,2})/2$ parts of pair momentum. In the paper, the decomposition of Pratt-Bertsch [3, 4] is used for $\vec{q}$ as well as the longitudinal comoving system (LCMS) frame. The volume of source can be written as follows:

$$V = (2\pi)^{3/2} R_s^2 R_l. \quad (3)$$

Comparison of (3) with definition from [5] is discussed in detail in [6]. One of the important additional observables is the following difference [7, 8]:

$$\delta \equiv R_o^2 - R_s^2. \quad (4)$$

If the emission function features no position-momentum correlation, then δ is finite at nonzero $\vec{K}$ only due to explicit $\vec{K}$-dependence (resulting from the mass-shell constraint $q^0 = \vec{q}\vec{K}/K^0$) [7]. In this case

$$\delta \approx \beta_{\perp}^2 (\Delta\tau)^2, \quad (5)$$

where $\beta_{\perp} = k_{\perp}/m_{\perp}$ is the transverse velocity of pair of particles with mass m, $m_{\perp}^2 = k_{\perp}^2 + m^2$, and $\Delta\tau$ is the emission duration for the particle type under discussion. It should be stressed that the last relation is valid in some specific cases of 1D hydrodynamics while it is violated in both the cascade approaches and multidimensional hydrodynamic models. Thus, in the framework of some assumptions, δ gives direct access to the emission duration of the source and allows us to partially disentangle the spatial and time information contained in radii parameters R_{ij} [7]. The sensitivity to the $\Delta\tau$ is the main advantage of the observable (4).

In the paper, the following set of main HBT observables $\mathcal{G}_1 \equiv \{\mathcal{G}_1^i\}_{i=1}^4 = \{\lambda, R_s, R_o, R_l\}$ is under consideration as well as the set of some important additional observables which can be calculated with help of HBT radii $\mathcal{G}_2 \equiv \{\mathcal{G}_2^j\}_{j=1}^3 = \{R_o/R_s, \Delta\tau, V\}$. The set of parameters $\mathcal{G}_1$ characterizes the chaoticity of source and its 4-dimensional geometry at freeze-out stage completely. Scaled parameters $\mathcal{G}_1^i$, $i = 2$–4, δ, and $\mathcal{G}_2^3$ are calculated as follows [1]:

$$R_i^n = \frac{R_i}{R_A}, \quad i = s,o,l; \quad \delta^n = \frac{\delta}{R_A^2}; \quad V^n = \frac{V}{V_A}. \quad (6)$$

Here $R_A = r_0 A^{1/3}$ and $V_A = 4\pi R_A^3/3$ are radius and volume of spherically symmetric nucleus, $r_0 = (1.25 \pm 0.05)$ fm [9, 10]. The change $R_A \rightarrow \langle R_A \rangle = (R_{A_1} + R_{A_2})/2$ is made in the relation (6) in the case of asymmetric nucleus-nucleus collisions [1]. One needs to emphasize that the most central collisions are usually used for studying the space-time characteristics of final-state matter and, in particular, for discussion of global energy dependence of HBT observables (see Section 3). Thus, the using of radius of all the nuclei in (6) seems reasonable. In general case the scale factor in (6) for calculation of scaled HBT radii, δ and volume should takes into account the centrality of nucleus-nucleus collisions. The normalization procedure suggested in [1] allows us to consider two data samples, namely, (i) only (quasi) symmetric heavy ion collisions and (ii) all available data for nucleus-nucleus collisions. Experimental data sets analyzed here are discussed in detail elsewhere [1, 6].

3. Energy Dependence of Space-Time Extent of Emission Region

Dependencies of HBT parameters $\mathcal{G}_1^i(\sqrt{s_{NN}})$, $i = 1$–4, and $R_o/R_s(\sqrt{s_{NN}})$ are shown in Figures 1(a)–1(d) and Figure 1(e), respectively. The chaoticity parameter λ decreases with increasing $\sqrt{s_{NN}}$ rapidly at lower (AGS) energies and shows the weak changing at $\sqrt{s_{NN}} > 4$ GeV (Figure 1(a)). HBT radii of source in transverse plane with respect to the beam direction, R_s (Figure 1(b)) and R_o (Figure 1(c)), show little change over a wide range of energies $5 \lesssim \sqrt{s_{NN}} \lesssim 200$ GeV which corresponds to the highest AGS, SPS, and RHIC beam collision energies. On the other hand, the value of source size in longitudinal direction, R_l (Figure 1(d)), appears to reach a minimum around $\sqrt{s_{NN}} = 5$ GeV, rising in energy domain available at RHIC. As seen there is increasing of HBT radii (Figures 1(b)–1(d)) at growth of collision energy from $\sqrt{s_{NN}} \sim 20$ GeV up to the maximum available LHC energy $\sqrt{s_{NN}} = 2.76$ TeV. The significant increasing of HBT radii is seen for much broader energy range (on about two orders of magnitude $\sqrt{s_{NN}} \sim 0.02$–3 TeV) only than was expected early at the beginning of RHIC operation. Therefore, the space-time extent of emission region at freeze-out changes slowly with increasing of collision energy. The transverse radius R_s reflects the spatial extent of particle source, whereas R_o is also affected by dynamics [12, 13] and is believed to be related to the duration of particle emission [14]. As indicated, for example, in [15], the ratio R_o/R_s was predicted to increase with beam energy by hydrodynamical calculations and might show a significant enhancement if the lifetime of the collision evolution (and, within these models, the duration of particle emission as a result) was to be extended by entrance into a different phase [14]. There is no significant increasing of ratio R_o/R_s in all experimentally available energy domains (Figure 1(e)). Recent developments, in particular in viscous hydrodynamics, allow us to get reasonable agreement between experimental and model values of R_o/R_s at top RHIC energy and demonstrate that the behavior of experimental dependencies of R_o/R_s on kinematic variables can be explained in particular by realistic EoS with crossover
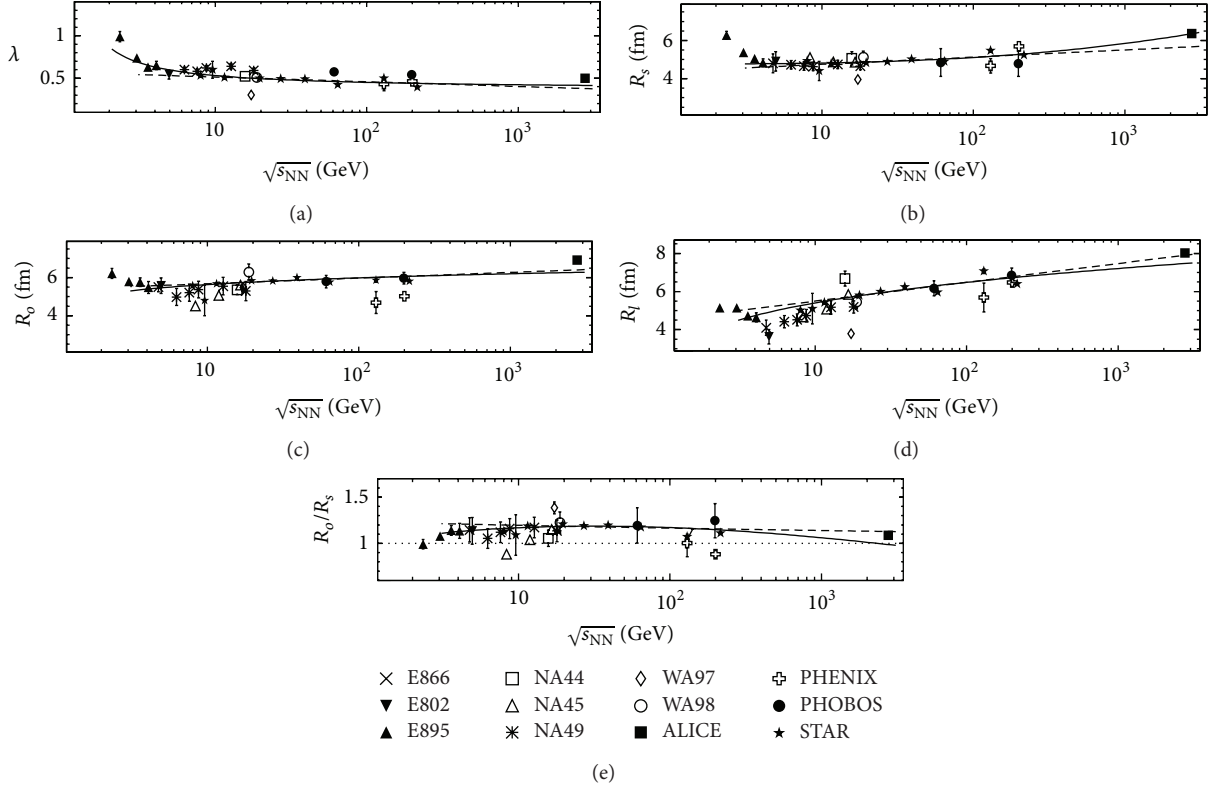
FIGURE 1: Dependence of chaoticity parameter (a), HBT radii (b–d), and ratio R_o/R_s (e) on collision energy for central heavy ion Au + Au, Au + Pb, Pb + Pb interactions at midrapidity and $\langle k_\perp \rangle \simeq 0.2$ GeV/c [6]. Experimental results are demonstrated for pairs of π^- mesons (in the cases of ALICE and STAR at $\sqrt{s_{NN}} = 7.7$–62.4 and 200 GeV, for $\pi^\pm\pi^\pm$ pairs) and for standard Coulomb correction $P_C^{(1)}(q)$ (in the cases of ALICE, NA44, NA45, PHOBOS, and STAR at $\sqrt{s_{NN}} = 7.7$, 11.5–62.4 and 200 GeV, for correction $P_C^{(3)}$). Statistical errors are shown (for NA44, total uncertainties). The solid lines (a–d) correspond to the fits by function (7) and dashed lines to the fits by specific case $\mathscr{G}_1^i \propto \ln \varepsilon$, $i = 1$–4. Fitted data samples for λ (a) and for R_l (d) do not include the point of the WA97 experiment [11], while the fits for transverse HBT radii (b, c) are shown for samples with point from [11]. Smooth solid and dashed curves at (e) correspond to the ratio R_o/R_s calculated from the fit results for R_s and R_o, and dotted line is the level $R_o/R_s = 1$.

phase transition and sQGP at high temperatures [16–21]. Therefore, the soft HBT observables confirm the phase transition and creation of deconfinement state of strongly interacting matter in collider experiments.

Taking into account the view of experimental dependencies in Figures 1(a)–1(d), the following function is suggested:

$$f\left(\sqrt{s_{NN}}\right) = a_1 \left[1 + a_2 \left(\ln \varepsilon\right)^{a_3}\right] \qquad (7)$$

for smooth approximation of $\mathscr{G}_1^i(\sqrt{s_{NN}})$, $i = 1$–4, where $\varepsilon \equiv s_{NN}/s_0$, $s_0 = 1$ GeV^2. Also the specific case of (7) at $a_3 = 1.0$ is under consideration. As seen from Figures 1(b)–1(d), there is indication on change of behavior of energy dependence (inflection point) for $\{\mathscr{G}_1^i\}_{i=2}^4$ at $\sqrt{s_{NN}} \simeq 5$ GeV. This inflection point is seen most clearly for R_l (Figure 1(d)). Therefore, the fit function (7) is used for approximation of the energy dependence of HBT radii in the energy domain $\sqrt{s_{NN}} \geq 5$ GeV only. Experimental energy dependence of λ is fitted by general function (7) at all available energies. As seen the point from the WA97 experiment [11] differs significantly from other results at close energies for λ (Figure 1(a)) and longitudinal radius (Figure 1(d)). Thus, for these parameters fits are made for data sample (i) with exception of the

point from [11]. For each main HBT parameter $\{\mathscr{G}_1^i\}_{i=1}^4$ fits are made for both the statistical and total errors, where total errors of experimental points include available clear indicated systematic errors added in quadrature to statistical ones. The numerical values of fit parameters are presented in Table 1, where the second line for each HBT parameter $\{\mathscr{G}_1^i\}_{i=1}^4$ corresponds to the approximation by specific case of (7). Fit curves are shown in Figure 1 by solid lines for (7) and by dashed lines for specific case of fit function at $a_3 = 1.0$ taking into account the statistical errors. In general, fit function described above agrees reasonably with experimental dependence $\mathscr{G}_1^i(\sqrt{s_{NN}})$, $i = 1$–4 (Figures 1(a)–1(d)). But the fit qualities are poor for all the main HBT parameters, especially for λ, with inclusion of the statistical errors only (Table 1). Spread of experimental points leads to the statistically unacceptable values of χ^2/n.d.f. In the case of λ inclusion of estimation for systematic uncertainty for Pb + Pb collisions at $\sqrt{s_{NN}} = 2.76$ TeV leads to both the dramatic growth of a_2 and improvement of the fit quality at transition from statistical errors of experimental points to total errors in data sample (i) (Table 1). Inclusion of total errors allows us to get statistically acceptable fit qualities for HBT radii

TABLE 1: Values of fit parameters for approximation of the data sample (i).

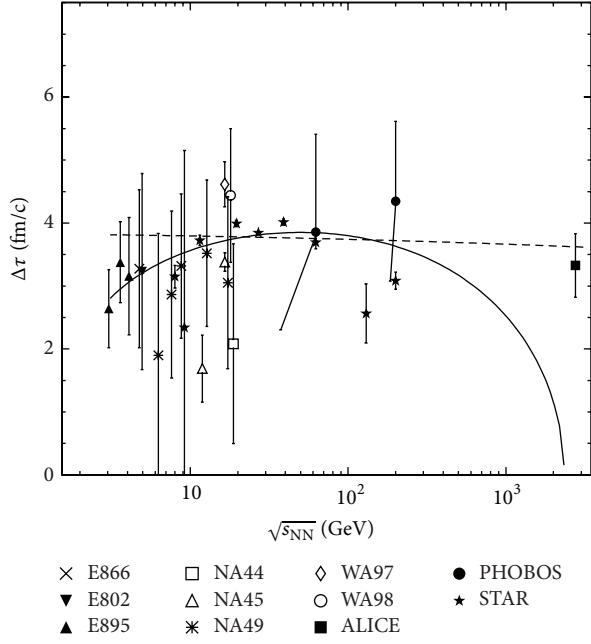| HBT parameter	Fit with statistical errors				Fit with total errors			
	a_1	a_2	a_3	χ^2/n.d.f.	a_1	a_2	a_3	χ^2/n.d.f.
λ	0.36 ± 0.02	1.90 ± 0.12	-0.91 ± 0.14	$534/23$	0.008 ± 0.002	104 ± 21	-0.291 ± 0.011	$373/23$
	0.570 ± 0.004	-0.021 ± 0.001	1.0 (fixed)	$580/19$	0.621 ± 0.005	-0.032 ± 0.001	1.0 (fixed)	$266/19$
R_s	4.77 ± 0.02	$(1.3 \pm 0.8) \times 10^{-4}$	2.8 ± 0.2	$141/22$	4.5 ± 0.2	$(1 \pm 2) \times 10^{-3}$	2.3 ± 0.9	$51.1/22$
	4.37 ± 0.03	0.0188 ± 0.0012	1.0 (fixed)	$194/23$	3.88 ± 0.18	0.038 ± 0.008	1.0 (fixed)	$54.5/23$
R_o	0.59 ± 0.06	7.4 ± 1.0	0.097 ± 0.009	$392/22$	0.64 ± 0.11	7 ± 2	0.03 ± 0.03	$31.9/22$
	5.38 ± 0.04	0.0120 ± 0.0012	1.0 (fixed)	$411/23$	5.3 ± 0.2	0.003 ± 0.002	1.0 (fixed)	$31.9/23$
R_l	0.110 ± 0.015	32 ± 4	0.267 ± 0.008	$357/21$	0.03 ± 0.03	87 ± 64	0.33 ± 0.03	$23.3/21$
	4.51 ± 0.04	0.0475 ± 0.0018	1.0 (fixed)	$459/22$	4.0 ± 0.2	0.065 ± 0.010	1.0 (fixed)	$26.3/22$

FIGURE 2: Energy dependence of emission duration for secondary charged pions in central heavy ion collisions Au+Au, Au+Pb, Pb+Pb in midrapidity region and at $\langle k_\perp \rangle \simeq 0.2\,\mathrm{GeV}/c$. Experimental results are shown for the same particle types and Coulomb corrections as well as in Figure 1. Error bars are only statistical (for NA44, total uncertainties). Smooth curves are derived from (5) and the fit results for R_s, R_o without the point of the WA97 experiment [11]. The solid line corresponds to the fits of HBT radii by function (7) and dashed line to the fits by specific case $R_i \propto \ln \varepsilon$, $i = s, o$.
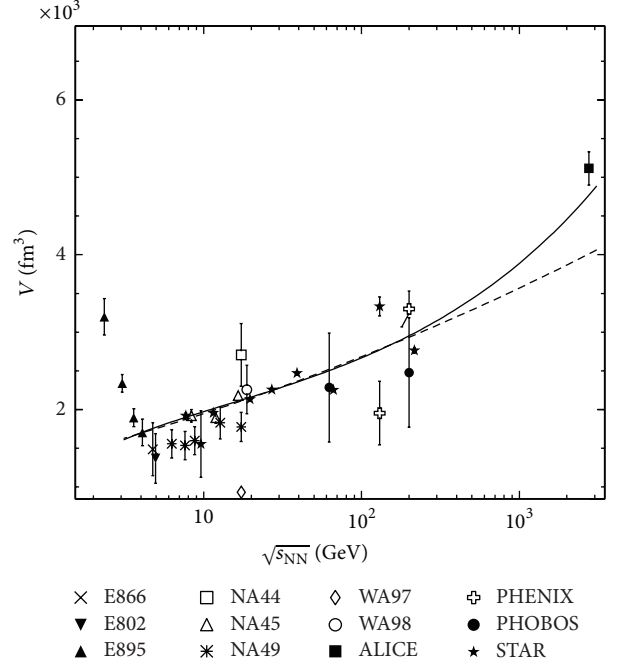

FIGURE 3: Energy dependence of volume of emission region at freeze-out for secondary charged pions in central heavy ion collisions Au + Au, Au + Pb, Pb + Pb in midrapidity region and at $\langle k_\perp \rangle \simeq 0.2\,\mathrm{GeV}/c$. Equation (3) is used for calculation of volume values. Experimental results are shown for the same particle types and Coulomb corrections as well as in Figure 1. Error bars are only statistical (for NA44, total uncertainties). Smooth curves are derived from (3) and the fit results for R_s, R_l taking into account the point of the WA97 experiment [11]. The solid line corresponds to the fits of HBT radii by function (7) and dashed line to the fits by specific case $R_i \propto \ln \varepsilon$, $i = s, l$.

for both function (7) and its specific case. It seems that a more complex fit function should be used in order to describe energy dependence of HBT radii at all available collision energies. This study is in progress. Taking into account the similar behavior of the energy dependence of HBT radii (Figures 2(b)–2(b)) and elliptic flow v_2 [22] at qualitative level the following functional form can be suggested: $g(\sqrt{s_{\mathrm{NN}}}) = a_1 + a_2(\sqrt{\varepsilon} - a_3)^{a_4} + \sum_{i=5,6} a_i \varepsilon^{a_{i+1}} + a_9(\ln \varepsilon)^{a_{10}}$, as first approach for description of $\mathscr{G}_1^i(\sqrt{s_{\mathrm{NN}}})$, $i = 1$–4, in all experimentally available energy domains. Smooth solid and dashed curves shown in Figure 1(e) are calculated for the ratio R_o/R_s from the fit results for R_s and R_o (Table 1). As seen these curves agree with experimental points reasonably at $\sqrt{s_{\mathrm{NN}}} \geq 5\,\mathrm{GeV}$. In general, fits by function (7) at free a_3 and fixed a_3 show close behavior for all the main HBT parameters from $\mathscr{G}_1$ with some differences at intermediate ($\sqrt{s_{\mathrm{NN}}} \lesssim 10\,\mathrm{GeV}$) and high ($\sqrt{s_{\mathrm{NN}}} > 200\,\mathrm{GeV}$) energies. These differences result in more significant discrepancy between fit curves for R_o/R_s (Figure 2(e)) and for other parameters from the set $\mathscr{G}_2$ (see discussion below).

Figure 2 demonstrates the energy dependence of $\Delta\tau$ for (quasi) symmetric heavy ion collisions. The emission duration in these collisions is calculated based on known HBT radii (Figures 1(b)–1(d)), kinematic regime for pion pairs, and (5). The $\langle \beta_\perp \rangle \approx 0.82$ for pion pairs with $\langle k_\perp \rangle \simeq 0.2\,\mathrm{GeV}/c$. Value $\Delta\tau = (0.53 \pm 9.15)\,\mathrm{fm}/c$ at $\sqrt{s_{\mathrm{NN}}} = 130\,\mathrm{GeV}$

derived from the PHENIX results at this energy is not shown due to extremely large errors. As seen the emission duration of pions extracted from δ is about 2–4 fm/c for any energies under consideration. The visible energy dependence of emission duration is absent, and $\Delta\tau(\sqrt{s_{\mathrm{NN}}})$ is close to flat within large error bars. One can see more interesting behavior for this dependence for the STAR high-statistics data [15] only. But additional precise measurements are necessary in order to confirm the change of $\Delta\tau(\sqrt{s_{\mathrm{NN}}})$ at $\sqrt{s_{\mathrm{NN}}} \sim 10$–20 GeV and locate the possible knee in the experimental dependence. Smooth solid and dashed curves shown in Figure 2 are calculated for $\Delta\tau$ from the fit results for R_s and R_o (Table 1). It seems that function (7) at free a_3 agrees better with experimental points at $\sqrt{s_{\mathrm{NN}}} \leq 200\,\mathrm{GeV}$ than that at fixed a_3. But large error bars do not allow the choice for preferable curve unambiguously. Moreover, the general function (7) underestimates $\Delta\tau$ in TeV-region significantly. Volume of the homogeneity region in various heavy ion collisions is calculated based on (3) and known HBT radii which are shown in Figures 1(b)–1(d). The energy dependence of estimations for volume of emission region is shown in Figure 3. Detailed comparison of the results for various definitions of V as well as for different sets of
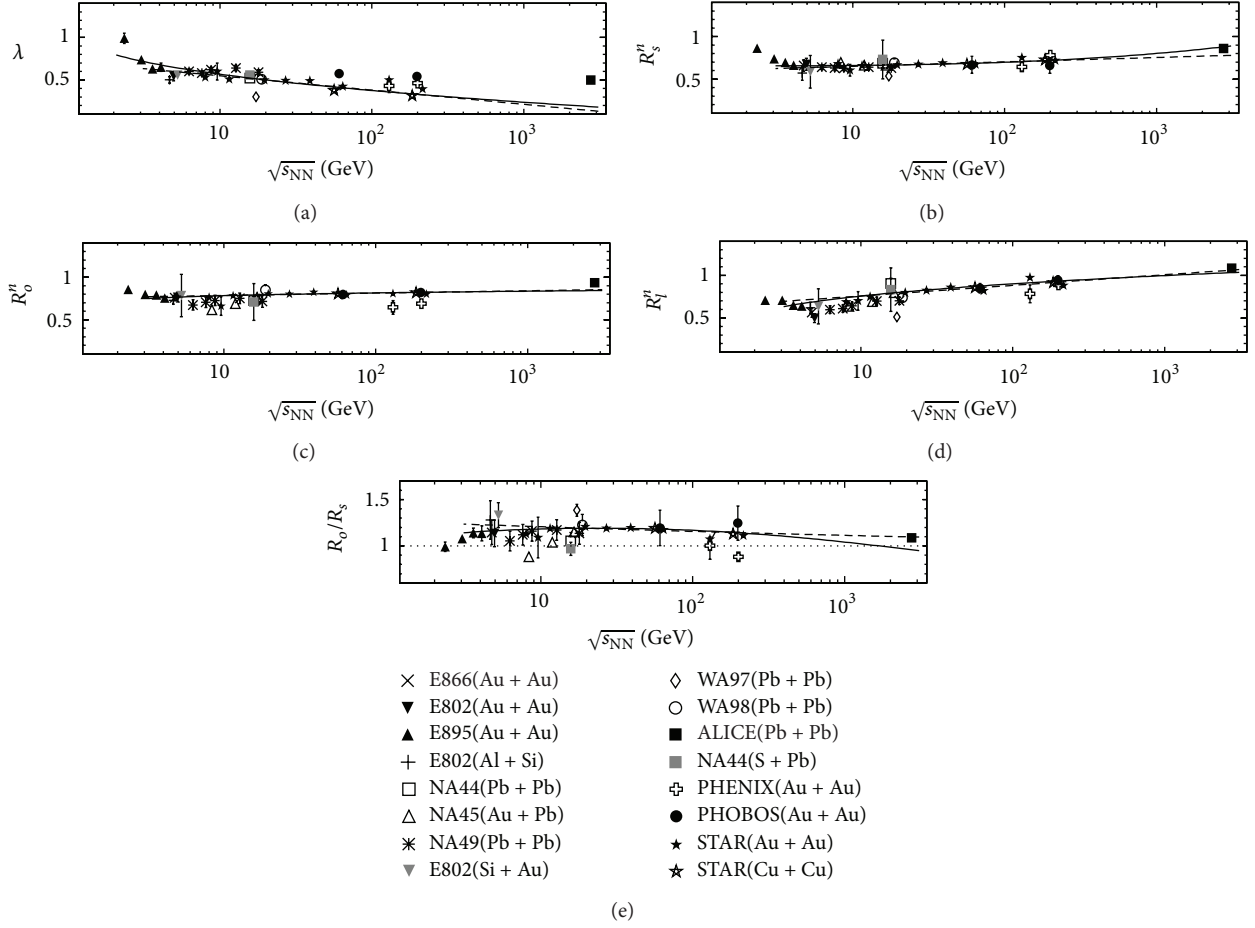
FIGURE 4: Energy dependence of λ parameter (a), scaled HBT radii (b–d), and ratio R_o/R_s (e) in various nucleus-nucleus collisions at $\langle k_\perp \rangle \simeq$ 0.2 GeV/c [6]. Experimental results are shown for central collisions (for minimum bias event in the case of E802 for Al + Si), for pairs of π^- mesons (in the cases of ALICE and STAR for both Cu + Cu and Au + Au at $\sqrt{s_{NN}} = 7.7$–62.4 and 200 GeV for $\pi^\pm \pi^\pm$ pairs, E802 for Al + Si, and NA44 for S + Pb, for pairs of π^+ mesons), and for standard Coulomb correction $P_C^{(1)}(q)$ (in the cases of ALICE, NA44, NA45, PHOBOS, and STAR for both Cu + Cu and Au + Au at $\sqrt{s_{NN}} = 7.7, 11.5$–62.4 and 200 GeV, for correction $P_C^{(3)}$). Statistical errors are shown (for NA44, total uncertainties). The solid lines (a–d) correspond to the fits by function (7) and dashed lines to the fits by specific case of (7) at fixed $a_3 = 1.0$. Smooth solid and dashed curves at (e) correspond to the ratio R_o/R_s calculated from the fit results for R_s^n and R_o^n, and dotted line is the level $R_o/R_s = 1$.

STAR data is discussed elsewhere [6]. Smooth solid and dashed curves shown in **Figure 3** are calculated for V from (3) and the fit results for R_s, R_l (**Table 1**). Both curves are very close at $\sqrt{s_{NN}} \leq 200$ GeV but function (7) at $a_3 = 1.0$ underestimates V in TeV-region significantly. Therefore, the general function (7) is the preferable approximation of the experimental $V(\sqrt{s_{NN}})$ at $\sqrt{s_{NN}} \geq 5$ GeV.

Predictions for values of the HBT observables from sets $\mathcal{G}_m$, $m = 1, 2$, are obtained for heavy ion mode energies of the LHC and the FCC project based on the fit results for the main HBT parameters. Estimations are shown in **Table 2** for fits with inclusion of statistical errors, and the second line for each collision energy corresponds to the using of the specific case of (7). Large uncertainties obtained for estimations based on function (7) do not allow us to distinguish predictions from (7) with free a_3 and with fixed $a_3 = 1.0$. One can expect the volume of homogeneity region $V \sim 6000$ fm^3 at $\sqrt{s_{NN}} = 5.52$ TeV (LHC) and $V \sim 9000$ fm^3 at $\sqrt{s_{NN}} = 39.0$ TeV (FCC)

based on the reasonable agreement between experimental data and solid curve in **Figure 3**.

Figure 4 shows the energy dependence of λ (a), scaled HBT radii (b–d), and R_o/R_s ratio (e) for both the symmetric and asymmetric collisions of various nuclei. Fits of experimental dependencies for the data sample (ii) are made by (7) in the same energy domains and with the same error types as well as for the data sample (i) and are shown in **Table 2**. It seems that the λ value from the WA97 experiment [11] cannot be excluded from the data sample (ii) because there are the STAR results $\lambda \sim 0.3$ for Cu + Cu collisions also (**Figure 4(a)**). There are no physics reasons in order to exclude the points of these experiments from the fitted data sample (ii) in the case of all available nucleus-nucleus collisions. Furthermore, the scaled value of longitudinal radius R_l^n from [11] agrees better with results of other experiments at close energies (**Figure 4(d)**) than that for the data sample (i). Therefore, there is no exception of any experimental point

TABLE 2: Estimations for observables based on fit results for the data sample (i).

$\sqrt{s_{NN}}$, TeV	λ	R_s, fm	R_o, fm	HBT parameter R_l, fm	R_o/R_s	$\Delta\tau$, fm/c	$V \times 10^{-3}$, fm^3
5.52	0.41 ± 0.03	6.8 ± 1.9	6.3 ± 1.0	7.6 ± 1.5	0.9 ± 0.3	—	6 ± 3
	0.362 ± 0.009	5.79 ± 0.10	6.49 ± 0.12	8.20 ± 0.16	1.12 ± 0.03	3.6 ± 0.4	4.33 ± 0.17
39.0	0.40 ± 0.02	8 ± 3	6.4 ± 1.0	8.0 ± 1.6	0.8 ± 0.3	—	9 ± 8
	0.315 ± 0.011	6.11 ± 0.12	6.74 ± 0.15	9.04 ± 0.19	1.10 ± 0.03	3.5 ± 0.5	5.3 ± 0.2

from fitted ensemble for any HBT observable in Figure 4 in contrast with the fitting procedure for the data sample (i). The numerical values of fit parameters are presented in Table 3, where the second line for λ and each normalized HBT radius correspond to the approximation by specific case of (7). Fit curves are shown in Figure 4 by solid lines for (7) and by dashed lines for specific case of fit function at $a_3 = 1.0$ taking into account statistical errors. Fit qualities are improved for R_s^n in the case of total errors of experimental point and for R_o^n at any error types of experimental point with respect to the corresponding fit results for the data sample (i) shown in Table 1. There is dramatic growth of $\chi^2/\text{n.d.f.}$ values for fits of λ data (Figure 4(a)) despite the qualitative agreement between smooth approximations and experimental λ values for range $10 \lesssim \sqrt{s_{NN}} \lesssim 200$ GeV. The fit by (7) at $a_3 = 1.0$ underestimates the λ value at the LHC energy $\sqrt{s_{NN}} = 2.76$ TeV significantly. The λ values for asymmetric nucleus-nucleus collisions at intermediate energies $\sqrt{s_{NN}} \lesssim 20$ GeV agree well with values of λ in symmetric heavy ion collisions at close energies. On the other hand, the λ for Cu + Cu collisions is smaller systematically than λ in Au + Au collisions in energy range $\sqrt{s_{NN}} = 62$–200 GeV (Figure 4(a)). New experimental data are important for verification of the suggestion of separate dependencies $\lambda(\sqrt{s_{NN}})$ for moderate and heavy ion collisions. Also the development of some approach is required in order to account for type of colliding beams in the case of λ parameter and improve quality of smooth approximation. In this case, significant growth of a_2 as well as improvement of the fit quality at transition from statistical errors of experimental points to total errors in the data sample (ii) (Table 3) is dominated by inclusion of estimations for systematic uncertainties for Cu + Cu collisions and/or Pb + Pb ones at $\sqrt{s_{NN}} = 2.76$ TeV. Smooth curves for scaled HBT radii and ratio R_o/R_s are in reasonable agreement with experimental dependencies in fitted domain of collision energies $\sqrt{s_{NN}} \geq 5$ GeV (Figures 4(b)–4(e)). Parameter values obtained for fit of R_l^n with total uncertainties by (7) at $a_3 = 1.0$ are equal within errors with results from [23] accounting for the fact that experimental results studied here are obtained at $\langle m_\perp \rangle \simeq 1.75 m_\pi$. Dramatic improvement of the fit qualities for scaled HBT radii at transition from the data sample (ii) with statistical errors to the data sample with total errors (Table 3) is dominated mostly by the uncertainty in r_0 that leads to additional errors due to scaling (6). At the same time inclusion of total uncertainties for Au + Au collisions at $\sqrt{s_{NN}} = 19.6$ GeV results in significant decreasing of a_2 parameter in the case of R_l^n scaled radius.

The corresponding dependencies for δ^n and V^n are demonstrated in Figures 5 and 6, respectively. And in [1] results for $\pi^+\pi^+$ pairs are shown in Figures 4–6 also because HBT parameters from the set $\mathcal{G}_1$ depend on sign of electrical charge of secondary pions weakly. Relation $R_o < R_s$ is observed for $\approx 11\%$ of points in Figure 5. In general the $\delta < 0$ can be possible in the model of opaque source with surface dominated emission [24, 25]. But possibly results should be similar for both the same ion beams and close kinematic regimes in various experiments. Therefore, additional study is required in order to distinguish the physical and technique
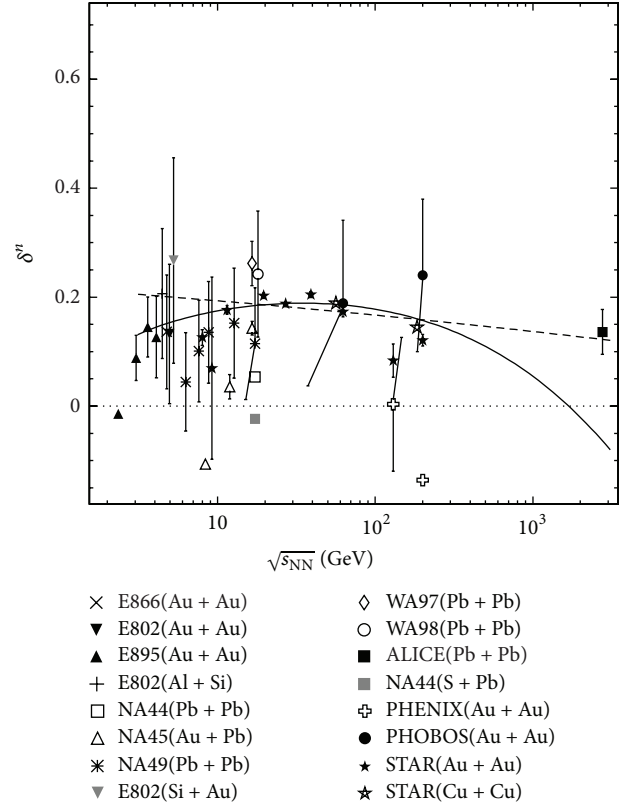

FIGURE 5: Dependence of scaled difference of squares of transverse radii on collision energy for emission region of secondary charged pion in various nucleus-nucleus collisions at $\langle k_\perp \rangle \simeq 0.2$ GeV/c. Experimental results are shown for the same particle types and Coulomb corrections as well as in Figure 4. Error bars are only statistical (for NA44, total uncertainties). Dotted line is the level $\delta^n = 0$. Smooth curves are derived from (6) and the fit results for R_s^n, R_o^n. The solid line corresponds to the fits of scaled HBT radii by function (7) and dashed line to the fits by specific case $R_i^n \propto \ln \varepsilon$, $i = s, o$.

sources of negative values of the δ^n in Figure 5 and to get a more definite explanation. The dependence $\delta^n(\sqrt{s_{NN}})$ is almost flat within large error bars in all energy domains under consideration. Taking into account the STAR high-statistics results [15] only one can see the indication on change of behavior of $\delta^n(\sqrt{s_{NN}})$ inside the range of collision energies $\sqrt{s_{NN}} = 11.5$–19.6 GeV. This observation is in agreement with features of behavior of emission duration dependence on $\sqrt{s_{NN}}$ (Figure 2) discussed above. The estimation of energy range agrees well with results of several studies [15, 26–31] in the framework of the phase-I of BES program at RHIC which indicate the transition from dominance of quark-gluon degrees of freedom to hadronic matter at $\sqrt{s_{NN}} \lesssim 19.6$ GeV. But future precise measurements are crucially important for extraction of more definite physics conclusions. Smooth solid and dashed curves shown in Figure 5 are calculated for δ^n from the fit results for R_s^n and R_o^n (Table 3). The situation is similar to that for $\Delta\tau$: calculation based on the fit function (7) at free a_3 agrees reasonably with experimental points at $\sqrt{s_{NN}} \leq 200$ GeV but underestimates δ^n in TeV-region significantly. The large errors in Figure 6 for strongly asymmetric

Table 3: Values of fit parameters for approximation of the data sample (ii).

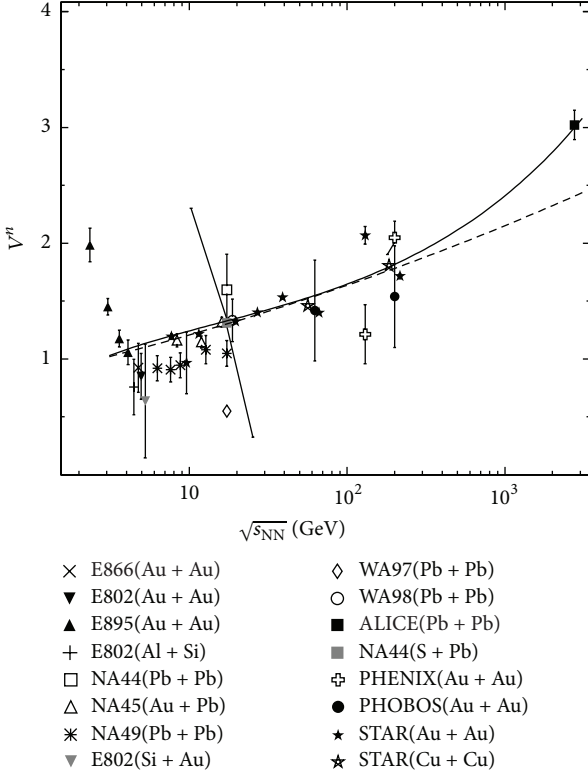| HBT parameter	Fit with statistical errors				Fit with total errors			
	a_1	a_2	a_3	χ^2/n.d.f.	a_1	a_2	a_3	χ^2/n.d.f.
λ	1.21 ± 0.09	-0.30 ± 0.04	0.38 ± 0.04	3656/29	0.60 ± 0.02	-0.014 ± 0.008	1.3 ± 0.2	780/29
	0.717 ± 0.003	-0.051 ± 0.001	1.0 (fixed)	3786/23	0.631 ± 0.005	-0.034 ± 0.001	1.0 (fixed)	706/23
R_s^n	0.656 ± 0.002	$(6 \pm 3) \times 10^{-5}$	3.11 ± 0.19	195/25	0.63 ± 0.02	$(6 \pm 5) \times 10^{-4}$	2.4 ± 0.9	26.8/25
	0.599 ± 0.003	0.019 ± 0.001	1.0 (fixed)	280/26	0.56 ± 0.03	0.029 ± 0.008	1.0 (fixed)	28.9/26
R_o^n	0.10 ± 0.02	6.3 ± 1.7	0.068 ± 0.006	402/25	0.019 ± 0.003	30 ± 9	0.12 ± 0.05	23.9/25
	0.758 ± 0.004	0.008 ± 0.001	1.0 (fixed)	415/26	0.67 ± 0.04	0.017 ± 0.008	1.0 (fixed)	24.4/26
R_l^n	0.022 ± 0.002	23 ± 3	0.258 ± 0.005	502/25	0.23 ± 0.04	0.8 ± 0.2	0.57 ± 0.05	66.0/25
	0.634 ± 0.004	0.043 ± 0.001	1.0 (fixed)	615/26	0.47 ± 0.03	0.089 ± 0.014	1.0 (fixed)	66.7/26

FIGURE 6: Energy dependence of scaled volume of emission region at freeze-out for secondary charged pions in various nucleus-nucleus collisions at $\langle k_\perp \rangle \simeq 0.2\,\text{GeV}/c$. Equation (3) is used for calculation of volume values. Experimental results are shown for the same collision, particle, and Coulomb correction types as well as in Figure 4. Error bars are only statistical (for NA44, total uncertainties). Smooth curves are derived from (3) and the fit results for R_s^n, R_l^n. The solid line corresponds to the fits of scaled HBT radii by function (7) and dashed line to the fits by specific case $R_i^n \propto \ln \varepsilon$, $i = s, l$.

nuclear collisions are dominated by large difference of radii of colliding moderate and heavy nuclei and corresponding large uncertainty for $\langle R_A \rangle$. Smooth solid and dashed curves shown in Figure 6 are calculated for V^n from (3) and the fit results for R_s^n, R_l^n (Table 3). The fit results for scaled HBT radii obtained with general function (7) lead to very good agreement between smooth curve and experimental data in TeV-region in contrast with the curve obtained from corresponding fit results for (7) at $a_3 = 1.0$.

Estimations for λ, R_o/R_s, and scaled HBT parameters at the LHC and the FCC energies are shown in Table 4 for fits of various nucleus-nucleus collisions with inclusion of statistical errors, and the second line for each collision energy corresponds to the using of the specific case of (7) at $a_3 = 1.0$. All the smooth approximations discussed above predict amplification of coherent pion emission with significant decreasing of λ. Uncertainties are large for estimations obtained on the basis of results of fits by function (7) at free a_3. Thus, values of HBT observables in Table 4 are equal within errors for general and specific case of (7) at $\sqrt{s_{\text{NN}}} = 5.52\,\text{TeV}$

(LHC) and $\sqrt{s_{\text{NN}}} = 39.0\,\text{TeV}$ (FCC) as well as for estimations obtained on basis of the data sample (i) above.

The energy dependencies for sets $\mathcal{G}_m$, $m = 1, 2$, of HBT parameters taking into account the scaling relation (6) and the high-statistics STAR data [15] demonstrate reasonable agreement between values of parameters obtained for interactions of various ions (shown in Figures 4–6). The observation confirms the suggestion [1] that scaled HBT parameters allow us to unite the study of both the symmetric and asymmetric nucleus-nucleus collisions in the framework of united approach. This qualitative suggestion is confirmed indirectly by recent study of two-pion correlations in the collisions of the lightest nucleus (d) with heavy ion (Au) at RHIC. Estimations of space-time extent of the pion emission source in d + Au collisions at top RHIC energy [32] in dependence on kinematic observables (collision centrality, the mean transverse momentum for pion pairs) indicate similar patterns with corresponding dependencies in Au + Au collisions and indicate similarity in expansion dynamics in collisions of various systems (d + Au and Au + Au at RHIC, p + Pb, and Pb + Pb at LHC). The scaling results for some radii indicate that hydrodynamic-like collective expansion is driven by final-state rescattering effects [32]. On the other hand, the scaled HBT parameters allow us to get the common kinematic dependencies only without any additional information about possible general dynamic features in different collisions. Thus, the hypothesis discussed above is qualitative only. The future quantitative theoretical and phenomenological studies are essential for verification of general features of soft stage dynamics for different collisions at high energies.

4. Summary

The following conclusions can be obtained by summarizing the basic results of the present study.

Energy dependence is investigated for a range of all experimentally available initial energies and for estimations of the main HBT parameters from the set $\mathcal{G}_1$ (λ and radii) derived in the framework of Gauss approach as well as for the set of important additional observables $\mathcal{G}_2$ included ratio of transverse radii, emission duration (or δ), and HBT volume. There is no dramatic change of values of HBT parameters with increasing of $\sqrt{s_{\text{NN}}}$ in domain of collision energies $\sqrt{s_{\text{NN}}} \geq 5\,\text{GeV}$. The estimation of emission duration of pions is about 2–4 fm/c for any energies under consideration. The energy dependence is almost flat for both the emission duration and the δ^n parameter within large error bars. The indication on possible curve knee at $\sqrt{s_{\text{NN}}} \sim 10$–$20\,\text{GeV}$ obtained in the STAR high-statistics data agrees with other results in the framework of the phase-I of the beam energy scan program at RHIC. But additional precise measurements are crucially important at various $\sqrt{s_{\text{NN}}}$ in order to confirm this feature in energy dependence of additional parameters (R_o/R_s, $\Delta \tau$, δ^n).

Analytic function is suggested for approximation of energy dependence of main HBT parameters. The fit curves demonstrate qualitative agreement with experimental data for λ at all available collision energies and for both the

Table 4: Estimations for observables based on fit results for the data sample (ii).

| $\sqrt{s_{NN}}$, TeV | λ | HBT parameter | | | | | |
		R_s^n	R_o^n	R_l^n	R_o/R_s	δ^n	V^n
5.52	0.16 ± 0.19	0.9 ± 0.2	0.8 ± 0.3	1.06 ± 0.16	0.9 ± 0.4	-0.2 ± 0.6	3.5 ± 1.6
	0.091 ± 0.004	0.792 ± 0.009	0.860 ± 0.010	1.099 ± 0.013	1.086 ± 0.018	0.11 ± 0.02	2.59 ± 0.07
39.0	0.07 ± 0.21	1.2 ± 0.4	0.9 ± 0.3	1.11 ± 0.16	0.7 ± 0.3	-0.7 ± 1.1	6 ± 4
	—	0.836 ± 0.011	0.883 ± 0.012	1.205 ± 0.015	1.06 ± 0.02	0.08 ± 0.03	3.17 ± 0.09

absolute and scaled HBT radii in energy domain $\sqrt{s_{NN}} \geq$ 5 GeV. Reasonable fit qualities are obtained for HBT radii at approximation of experimental points with total errors. Smooth curves calculated for energy dependence of the set $\mathscr{G}_2$ of additional HBT parameters agree reasonably with corresponding experimental data in most cases. Estimations of HBT observables are obtained on the basis of the fit results for energies of the LHC and the FCC project. For multi-TeV energy domain the emission region of pions will be characterized by decreased chaoticity parameter, linear sizes about 8.5–9.5 fm in longitudinal direction and 7-8 fm in transverse plane, and volume of about 10^4 fm^3.

Conflict of Interests

The author declares that there is no conflict of interests regarding the publication of this paper.

References

[1] V. A. Okorokov, "Energy dependence of femtoscopy properties of pion source in nuclear collisions," http://arxiv.org/abs/1312.4269.

[2] Y. Sinyukov, "Boson spectra and correlations in small thermalized systems," in *Hot Hadronic Matter: Theory and Experiment*, J. Letessier, H. G. Gutbrod, and J. Rafelski, Eds., vol. 346 of *NATO ASI Series B*, pp. 309–322, Plenum, New York, NY, USA, 1995.

[3] S. Pratt, "Pion interferometry of quark-gluon plasma," *Physical Review D*, vol. 33, Article ID 1314, 1986.

[4] G. F. Bertsch, M. Gong, and M. Tohyama, "Pion interferometry in ultrarelativistic heavy-ion collisions," *Physical Review C*, vol. 37, Article ID 1896, 1988.

[5] V. A. Okorokov, "Strange particle femtoscopy in relativistic heavy ion collisions: experimental overview," in *Proceedings of the XVIII International Baldin Seminar on High Energy Physics Problems*, A. N. Sissakian, V. V. Burov, and A. I. Malakhov, Eds., p. 101, Dubna, Russia, 2008.

[6] V. A. Okorokov, "Azimuthally integrated HBT parameters for charged pions in nucleus-nucleus interactions versus collision energy," http://arxiv.org/abs/1409.3925.

[7] U. A. Wiedemann and U. Heinz, "Particle interferometry for relativistic heavy-ion collisions," *Physics Reports*, vol. 319, pp. 145–230, 1999.

[8] V. A. Okorokov and E. V. Sandrakova, *Fractals in Fundamental Physics. Fractal Properties of Multiparticle Production and Topology of Sample*, MEPhI, Moscow, Russia, 2009.

[9] L. Valentin, *Subatomic Physics: Nuclei and Particles*, V. I. Ermann, Paris, France, 1982.

[10] K. N. Mukhin, *Experimental Nuclear Physics*, Energoatomizdat, Moscow, Russia, 1983.

[11] F. Antinori, W. Beusch, I. J. Bloodworth et al., "Centrality dependence of the expansion dynamics in Pb-Pb collisions at 158 A GeV c^{-1}," *Journal of Physics G: Nuclear and Particle Physics*, vol. 27, no. 11, p. 2325, 2001.

[12] F. Retiére and M. A. Lisa, "Observable implications of geometrical and dynamical aspects of freeze-out in heavy ion collisions," *Physical Review C*, vol. 70, Article ID 044907, 2007.

[13] E. Mount, G. Graef, M. Mitrovski, M. Bleicher, and M. A. Lisa, "Correspondence between Hanbury-Brown–Twiss radii and

[14] G. F. Bertsch, "Pion interferometry as a probe of the plasma," *Nuclear Physics A*, vol. 498, pp. 173–179, 1989.

[15] L. Adamczyk, J. K. Adkins, G. Agakishiev et al., "Beam energy dependent two-pion interferometry and the freeze-out eccentricity of pions in heavy ion collisions at STAR," http://arxiv.org/abs/1403.4972.

[16] W. Broniowski, "Uniform description of soft observables in heavy-ion collisions $\sqrt{s_{NN}}$ = 200 GeV," *Physical Review Letters*, vol. 101, Article ID 022301, 2008.

[17] S. Pratt, "Resolving the Hanbury Brown-Twiss puzzle in relativistic heavy ion collisions," *Physical Review Letters*, vol. 102, Article ID 232301, 2009.

[18] I. A. Karpenko and Y. M. Sinyukov, "Energy dependence of pion interferometry scales in ultra-relativistic heavy ion collisions," *Physics Letters B*, vol. 688, no. 1, pp. 50–54, 2010.

[19] I. A. Karpenko and Y. M. Sinyukov, "Kaon and pion femtoscopy at the highest energies available at the BNL Relativistic Heavy Ion Collider (RHIC) in a hydrokinetic model," *Physical Review C*, vol. 81, Article ID 054903, 2010.

[20] K. Werner, I. Karpenko, T. Pierog, M. Bleicher, and K. Mikhailov, "Event-by-event simulation of the three-dimensional hydrodynamic evolution from flux tube initial conditions in ultrarelativistic heavy ion collisions," *Physical Review C*, vol. 82, Article ID 044904, 2010.

[21] P. Bozek, "Interferometry radii in heavy-ion collisions at $\sqrt{s}$ = 200 GeV and 2.76 TeV," *Physical Review C*, vol. 83, Article ID 044910, 2011.

[22] V. A. Okorokov, "Azimuthal anisotropy and fundamental symmetries in QCD matter at RHIC," in *Proceedings of the 13th International Conference on Selected Problems of Modern Physics (SPMTP '09)*, B. M. Barbashov and S. M. Eliseev, Eds., E1,2-2009-36, p. 201, Dubna, Russia, 2009.

[23] G. Alexander and I. Ben Mordechai, "On Bose–Einstein correlations in *AA* collisions versus energy, transverse mass and momentum," *Journal of Physics G: Nuclear and Particle Physics*, vol. 40, Article ID 125101, 2013.

[24] H. Heiselberg and A. P. Visher, "Bose-Einstein correlations from opaque sources," *The European Physical Journal C*, vol. 1, no. 3, pp. 593–597, 1998.

[25] L. McLerran and S. S. Padula, "R_{out}/R_{sid} and opacity at RHIC," http://arxiv.org/abs/nucl-th/0205028.

[26] L. Adamczyk, J. K. Adkins, G. Agakishiev et al., "Elliptic flow of identified hadrons in Au+Au collisions at $\sqrt{s_{NN}}$ = 7.7 − 62.4 GeV," *Physical Review C*, vol. 88, Article ID 014902, 2013.

[27] L. Adamczyk, "Observation of an energy-dependent difference in elliptic flow between particles and antiparticles in relativistic heavy ion collisions," *Physical Review Letters*, vol. 110, Article ID 142301, 2013.

[28] L. Adamczyk, J. K. Adkins, G. Agakishiev et al., "Energy dependence of moments of net-proton multiplicity distributions at RHIC," *Physical Review Letters*, vol. 112, Article ID 032302, 2014.

[29] L. Adamczyk, J. K. Adkins, G. Agakishiev et al., "Beam-energy dependence of the directed flow of protons, antiprotons, and pions in Au+Au collisions," *Physical Review Letters*, vol. 112, Article ID 162301, 2014.

[30] L. Adamczyk, J. K. Adkins, G. Agakishiev et al., "Beam energy dependence of moments of the net-charge multiplicity distributions in Au+Au collisions at RHIC," *Physical Review Letters*, vol. 113, Article ID 092301, 2014.

the emission zone in noncentral heavy ion collisions," *Physical Review C*, vol. 84, Article ID 014908, 2011.

[31] L. Adamczyk, J. K. Adkins, G. Agakishiev et al., "Beam-energy dependence of charge separation along the magnetic field in Au+Au collisions at RHIC," *Physical Review Letters*, vol. 113, Article ID 052302, 2014.

[32] A. Adare, S. Afanasiev, C. Aidala et al., "Comparison of the space-time extent of the emission source in d+Au and Au+Au collisions at $\sqrt{s_{NN}} = 200$ GeV," http://arxiv.org/abs/1404.5291.